RSC Advances

PAPER

View Article Online
View Journal | View Issue

Open Access Article. Published on 19 September 2017. Downloaded on 11/2/2025 11:16:51 PM.
This article is licensed under a Creative Commons Attribution 3.0 Unported Licence.

Check for updates

Cite this: *RSC Adv.*, 2017, 7, 44860

Revealing phase relations between Fe_2B_7 and FeB_4 and hypothetical Fe_2B_7-type Ru_2B_7 and Os_2B_7: first-principles calculations†

Yunkun Zhang,[a] Biao Wan,[ab] Lailei Wu,*[ac] Zhiping Li,[c] Zhibin Wang,[c] Jingwu Zhang,*[a] Huiyang Gou*[bc] and Faming Gao[c]

Received 24th July 2017
Accepted 6th September 2017

DOI: 10.1039/c7ra08134k

rsc.li/rsc-advances

Investigation of new materials recovered using high pressure can foresee the unobservable structures and bonding of crystals. Employing first-principles calculations, we aim to provide an atomic understanding of the origin of multiple phases and mutual intergrowth for metastable iron borides. The competing FeB_4 and Fe_2B_7 in the experiment are compared by their enthalpy and structural features. The closely similar enthalpy of Fe_2B_7 + B and Fe_2B_8 (FeB_4) may explain the coexistence and tight mutual intergrowth of these two phases. The hypothetical Ru_2B_7 and Os_2B_7 are also suggested by the stability evaluations. The stable Ru_2B_7 and Os_2B_7 show an interesting metallic property and a great mechanical property due to the hybridization of metal-d and B-p orbitals and B–B covalent bonding.

1 Introduction

Over the decades, transition metal (TM) borides have attracted much attention due to their great promise for hard, wear-resistant, chemically inert coatings' applications.[1–4] Extensive experimental and theoretical studies have been performed with a focus on the synthesis and physical property characterizations of transition metal borides. Thus far, a variety of transition metal borides, *e.g.* OsB_2,[5] RuB_2,[2] ReB_2,[2,6–10] WB_4,[2,11–13] and CrB_4,[14,15] have been successfully synthesized in experiments, enabling the discovery of structural complexity, unique chemical bonding and exotic properties. Subsequently, the Os–B, Ru–B and W–B systems were investigated by first-principles calculations and the stable phases with different stoichiometry were identified, providing a road map for exploring design and synthesis strategies for new osmium, ruthenium and tungsten borides.[16,17] Recently, FeB_4 with *Pnnm* symmetry was synthesized to be a phonon mediated superconductor.[18] Computational structure simulations of the energy landscape did expedite the exploration for the discovery of FeB_4.[19] Interestingly, Fe_2B_7 was found to coexist with FeB_4 in experiments. This stoichiometry was not previously identified in any 3d metal boron systems. Aided by single-crystal X-ray diffraction, Bykova *et al.*[20] identified Fe_2B_7 to have an orthorhombic symmetry of *Pbam*, with lattice parameters of $a = 16.9699(15)$ Å, $b = 10.6520(9)$ Å, and $c = 2.8938(3)$ Å. However, the understanding of this compound is lacking to date, although Fe_2B[21] and FeB_2 (ref. 22) in the Fe–B system have been theoretically reported. Moreover, an experimental determination of the phase stability of Fe_2B_7 and FeB_4 has not been characterized. Furthermore, FeB_4 is found to exhibit great incompressibility along the *b* axis.[18] Due to the intergrowth of Fe_2B_7 and FeB_4, Fe_2B_7 may exhibit interesting physical properties. In view of the similarity of these two borides, there is a lack of understanding of the mechanical and electronic properties of this phase. Knowledge about these properties is essential to the understanding of the fundamental phase behaviors of this compound and offers the potential to discover new phases in transition metal borides.

It is found that chemically related compounds usually share similar crystallographic structure.[23] OsB_2 and RuB_2 crystallize in the orthorhombic *Pmmn* structure.[24,25] Furthermore, OsN_2 and RuN_2 are also formed in the same marcasite structure.[26,27] In addition, IrN_2 was predicted to have the IrP_2-type structure by Wang *et al.*[28] It is thus reasonable to expect the existence of Ru_2B_7 and Os_2B_7 with the same crystal symmetry of Fe_2B_7. Inspired by the potential of investigating the rich phase space of metal borides, we carried out a systematic study of Fe_2B_7, Ru_2B_7 and Os_2B_7 based on first-principles density functional calculations. We elucidated their phase relations and discussed their thermodynamic stability and mechanical and electronic properties. The results may provide guidance for further experimental and theoretical studies of these phases.

[a]Key Laboratory of Metastable Materials Science and Technology, College of Material Science and Engineering, Yanshan University, Qinhuangdao 066004, China. E-mail: wll@ysu.edu.cn; zjw@ysu.edu.cn

[b]Center for High Pressure Science and Technology Advanced Research, Beijing 100094, China. E-mail: huiyang.gou@gmail.com

[c]Key Laboratory of Applied Chemistry, College of Environmental and Chemical Engineering, Yanshan University, Qinhuangdao 066004, China

† Electronic supplementary information (ESI) available. See DOI: 10.1039/c7ra08134k

This journal is © The Royal Society of Chemistry 2017

Open Access Article. Published on 19 September 2017. Downloaded on 11/2/2025 11:16:51 PM.
This article is licensed under a Creative Commons Attribution 3.0 Unported Licence.

2 Computational details and methods

The structural optimizations were performed within CASTEP code.[29] Exchange and correlation functional was treated by the generalized gradient approximation with Perdew–Burke–Ernzerhof (GGA-PBE).[30] An energy cutoff of 500 eV and dense k-point grids within the Monkhorst–Pack scheme[31] were adopted for the Brillouin zone sampling, yielding excellent convergence for total energies (within 1 meV per atom). By calculating the individual elastic constants of crystals, C_{ij}, bulk modulus, B, and shear modulus, G, were obtained using the Voight–Reuss–Hill (VRH) approximation.[32] The theoretical Vickers hardness was estimated using Chen's empirical model,[33] $H_v = 2.0(k^2G)^{0.585} - 3.0$, and Tian's empirical model,[34] $H_v = 0.92k^{1.137}G^{0.708}$, where $k = G/B$. In the enthalpy calculations, α-B and γ-B are adopted as the reference structure below 20 GPa and 20–50 GPa for boron, respectively.

Formation enthalpy was calculated by the following formula:

$$\Delta H = [H(TM_2B_7) - 2H(TM) - 7H(B)]/(2 + 7) \quad (1)$$

where TM represents transition-metal Ru and Os, and H is the enthalpy of a constituent element.

3 Results and discussion

Motivated by the tight mutual intergrowth of FeB_4 and Fe_2B_7 in the experiment, we initially examined the structural stability by calculating the relative enthalpy as a function of pressure, shown in Fig. 1. In the pressure range from 0 to 50 GPa, both Fe_2B_7 + B and Fe_2B_8 (FeB_4) are found to be favored with respect to element Fe and B phases. Moreover, the enthalpy of Fe_2B_7 + B is very similar to that of Fe_2B_8 (FeB_4) in the entire pressure range considered (the enthalpy difference is 9–14 meV per atom), which confirms the coexistence of Fe_2B_7 and FeB_4 during the synthesis process. Orthorhombic FeB was also obtained independent of pressure in their high-pressure experiments, and hence the relative enthalpy of Fe_2B_2 + 6B (FeB + B) is also shown for comparison. In the entire pressure range, the enthalpy of Fe_2B_2 + 6B (FeB + B) is lower than that of 2Fe + 8B, but higher than that of Fe_2B_7 + B and Fe_2B_8 (FeB_4). The larger enthalpy difference between Fe_2B_2 + 6B (FeB + B) and Fe_2B_8 (FeB_4) may explain why they are not in tight mutual intergrowth.

The structural characteristic of Fe_2B_7 with FeB_4 may give the clue of the phase competition of Fe_2B_7 and FeB_4 during

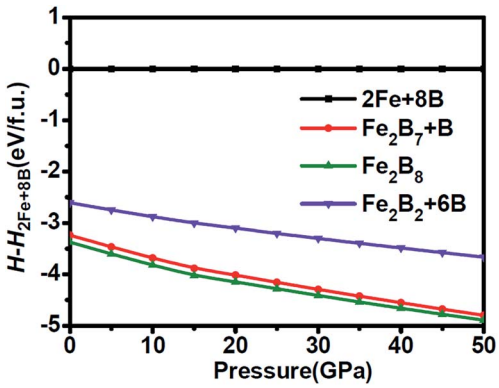

Fig. 1 Relative enthalpy of Fe_2B_7 + B, Fe_2B_8 and Fe_2B_2 + 6B with respect to 2Fe + 8B as a function of pressure.

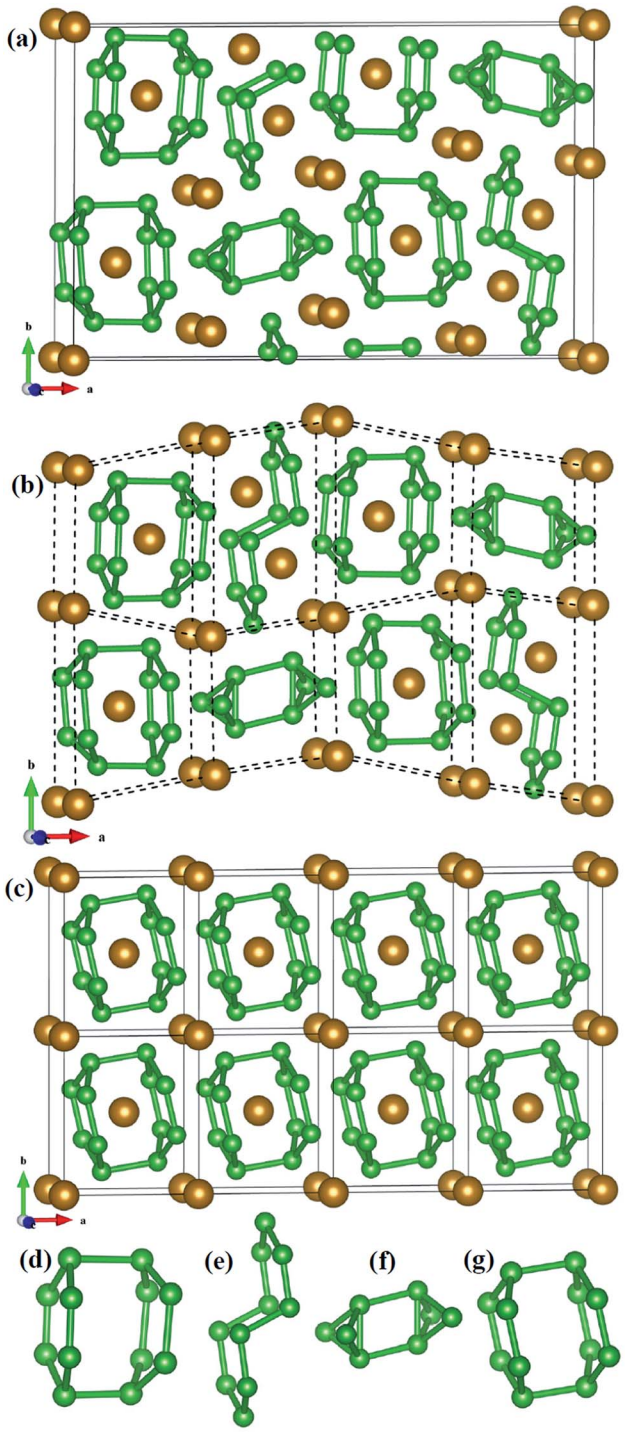

Fig. 2 (a) The unit cell of Fe_2B_7, (b) the unit cell of Fe_2B_7 can be seen as eight small cells, (c) 4 × 2 × 1 supercell of FeB_4, (d–f) B12, B10 and B8 units in Fe_2B_7, respectively, (g) B12 units in FeB_4. The brown and green spheres represent Fe and B atoms, respectively.

Open Access Article. Published on 19 September 2017. Downloaded on 11/2/2025 11:16:51 PM. This article is licensed under a Creative Commons Attribution 3.0 Unported Licence.

synthesis. As shown in Fig. 2a, the structure of Fe_2B_7 consists of B12, B10 and B8 units (see Fig. 2d–f), with Fe atoms situated among or inside these units. Therefore, each unit cell of Fe_2B_7 can be viewed as eight small distorted cells (see Fig. 2b). Compared with Fe_2B_7, FeB_4 (see Fig. 2c) consists of only B12 units (see Fig. 2g) with Fe atoms located inside. In Fe_2B_7, the length of B–B bonds is 1.616–2.028 Å in the B12 units, 1.666–1.771 Å in the B10 units, and 1.669–1.896 Å in the B8 units. For FeB_4, the length of B–B bonds is between 1.694 and 1.880 Å in the B12 units, which is close to the lengths of B–B bonds in B12, B10 and B8 units in Fe_2B_7. Between the two structures, moreover, we can find some close correlation that the size of the unit cell of Fe_2B_7 is closely similar to the size of the $4 \times 2 \times 1$ supercell of FeB_4. Therefore, we can speculate that the small cells with B12 units in Fe_2B_7 may transform to a unit cell of FeB_4 through compression, and on adding more B in the experiment, the small cells with B10 and B8 units in Fe_2B_7 may also transform to FeB_4 through diffusion and deformation (high pressure and temperature may be needed). Hence, it is reasonable to consider that FeB_4 may be synthesized by reacting Fe_2B_7 and B under certain conditions.

It is known that RuB_2 and OsB_2 crystallize in the same orthorhombic structure.[24,25] Similarly, RuN_2 and OsN_2 in experiment adopt an identical marcasite-type structure.[26,27] In addition, IrP_3,[35] $IrAs_3$,[36] $IrSb_3$,[36] CoP_3,[35] and RhP_3 (ref. 35) with cubic skutterudite $CoAs_3$-type structure were synthesized in experiments. Corresponding nitrides IrN_3,[37] CoN_3 (ref. 38) and RhN_3 (ref. 38) with the same type structure were also suggested by first-principles calculations. Thus, it is expected that Ru_2B_7 and Os_2B_7 adopt a similar crystallographic structure to *Pbam*-Fe_2B_7. The lattice parameters of Fe_2B_7, Ru_2B_7 and Os_2B_7 obtained from geometric optimization are listed in Table 1 in comparison with available experiment data. The calculated lattice parameters of *Pbam*-Fe_2B_7 are in good agreement with the experimental data within a maximum error of 1.4%, which confirms the reliability of our calculations.

In order to check the possibility of the existence of Ru_2B_7 and Os_2B_7, we calculated the formation enthalpy of the two phases. The computed formation enthalpy is −0.071 eV per atom for Ru_2B_7 and 0.058 eV per atom for Os_2B_7. However, at a pressure of 100 GPa, the formation enthalpy for Os_2B_7 becomes negative, with the value of −0.027 eV. The negative formation enthalpy indicates that Ru_2B_7 may exist at ambient pressure, while Os_2B_7 should be favored with high pressure.

The mechanical stability of the proposed Ru_2B_7 and Os_2B_7 is checked by calculating their individual elastic constants, as listed in Table 2. The calculated elastic constants fully satisfy Born–Huang stability criteria,[37] suggesting their mechanical stability. For comparison, the elastic constants of Fe_2B_7 are also given in Table 2, together with the bulk modulus B, shear modulus G, Young's modulus E, Poisson's ratio ν and Vickers hardness H_v. We can see that as the atomic number of TM (TM = Fe, Ru and Os) increases, the elastic constants C_{11}, C_{22} and C_{33} decrease. The C_{22} value for Fe_2B_7 is 691 GPa, slightly lower than that of *Pnnm*-FeB_4 (717 GPa).[39] For all three compounds TM_2B_7 (TM = Fe, Ru and Os), C_{22} is much larger than C_{11} and C_{33}, similar to that in VB_4,[40] CrB_4,[14] FeB_4 (ref. 39) and MnB_4,[41] as the shortest B–B bonds are almost parallel to the [010] direction. The calculated bulk modulus of Fe_2B_7 is 274 GPa, which is consistent with the experiment value of 268.9 GPa,[20] and higher than the experiment value of *Pnnm*-FeB_4 (252 GPa).[18] Although the valence electron density of element Ru and Os is higher than that of Fe, the bulk modulus of Ru_2B_7 and Os_2B_7 is only 264 GPa and 272 GPa, respectively, suggesting that the valence electron density is not a predominant factor accounting for the bulk moduli of TM_2B_7 (TM = Fe, Ru and Os) but the boron network. Moreover, Fe_2B_7 exhibits the highest shear modulus (197 GPa) and hardness (26.9 GPa), comparable to the theoretical value of *Pnnm*-FeB_4 (197.97 GPa/28.4 GPa). The G/B ratio, proposed by Pugh,[42] is correlated with the brittleness and ductility of materials ($G/B > 0.57$ corresponds to brittle and $G/B < 0.57$ to ductile behavior). Fe_2B_7 and Ru_2B_7 are brittle with G/B values of 0.72 and 0.60, while Os_2B_7 is ductile with a G/B ratio of 0.50. Poisson's ratio, ν, is an important parameter to describe the directional degree of covalent bonds in a material.[43] For Fe_2B_7, Ru_2B_7 and Os_2B_7, ν values are 0.21, 0.25 and 0.28, respectively, indicating their directional covalent bonding.

Young's modulus (E) is an important mechanical parameter to measure of the stiffness of a solid material. To get a better understanding of the direction oriented Young's modulus, a 3D representation and corresponding two dimensional (2D) projections of Young's modulus for Fe_2B_7, Ru_2B_7 and Os_2B_7 as a function of the crystallographic direction[44] are calculated and presented in Fig. 3. The shape deviation from a sphere indicates the degree of anisotropy in the system. Clearly, they all exhibit a slight elastic anisotropy, and the elastic anisotropy increases as the atomic radius of TM (TM = Fe, Ru and Os) increases. For Fe_2B_7, the 2D projections of Young's modulus in the *xy*, *xz* and *yz* planes have similar profiles, and the lowest Young's modulus values are along the [010] direction. For Ru_2B_7, the 2D projection of Young's modulus in the *xy* plane exhibits greater anisotropy than that in the *xz* and *yz* planes. For Os_2B_7, the lowest Young's modulus values are along the [100] direction, with the 2D projection of Young's modulus in the *xy* and *xz* planes showing larger anisotropy than in the *yz* plane.

The dynamical stability of the newly proposed Ru_2B_7 and Os_2B_7 is checked by calculating the phonon spectra (see ESI Fig. S1†). Both compounds are dynamically stable with no imaginary frequency found throughout the Brillouin zone.

To investigate the effect of the atomic radius of TM (TM = Fe, Ru and Os) on the electronic properties, we calculated the density of states (DOS) and band structure of Fe_2B_7, Ru_2B_7 and Os_2B_7, and the results are shown in Fig. 4. Due to the similarity of the crystal structure, the DOS profile of the three compounds

Table 1 Calculated equilibrium lattice parameters *a*, *b*, and *c* (Å) of Fe_2B_7, Ru_2B_7 and Os_2B_7, compared to available experiment data

	a	*b*	*c*	Ref.
Fe_2B_7	16.732	10.538	2.893	20
	16.9699	10.6520	2.8938	
Ru_2B_7	17.965	11.061	2.984	
Os_2B_7	18.322	11.101	2.989	

Table 2 Calculated elastic constants, C_{ij} (GPa), bulk moduli, B (GPa), shear moduli, G (GPa), Young's moduli, E (GPa), Poisson's ratio v and Vicker's hardness, H_v (GPa) for Fe_2B_7, Ru_2B_7 and Os_2B_7

	C_{11}	C_{22}	C_{33}	C_{44}	C_{55}	C_{66}	C_{12}	C_{13}	C_{23}	B	G	G/B	E	v	H_v (Chen)	H_v (Tian)
Fe_2B_7	396	691	432	240	205	237	148	172	183	274	197	0.72	477	0.21	26.9	26.6
Ru_2B_7	378	614	404	161	201	160	209	154	155	264	159	0.60	397	0.25	18.4	18.7
Os_2B_7	359	575	377	148	194	134	242	190	166	272	136	0.50	350	0.28	12.7	13.6

is quite similar to each other, the valence band is dominated by B-s states at low energy part, B-p states in the middle range, and TM (TM = Fe, Ru and Os)-d states at the higher energies. We observe the gradual shift of the main peak in the DOS to a lower energy region as the atomic radius of TM (TM = Fe, Ru and Os) increases. All three compounds exhibit metallic features due to the finite values at the Fermi level (E_F), which is mainly contributed by TM (TM = Fe, Ru and Os)-d state. The DOSs of TM (TM = Fe, Ru and Os)-d and B-p show a similar profile from the bottom of the valence band to the Fermi level, indicating the covalent hybridization between TM (TM = Fe, Ru and Os) and B atoms. Note that a pseudogap near the Fermi level is observed for all three compounds, enhancing their structural stability. In the band structure of these compounds, the large dispersion bands cross the Fermi level, also revealing their metallic character.

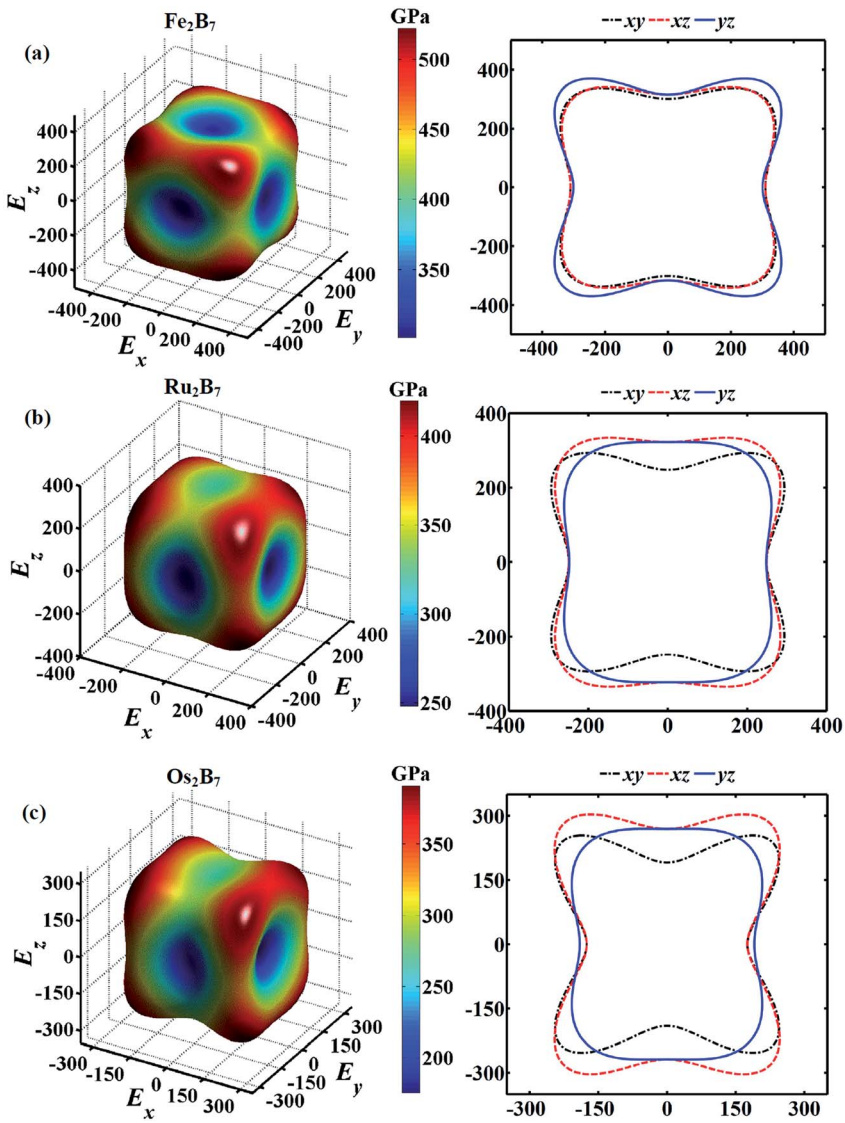

Fig. 3 3D representations and 2D projections of Young's moduli for (a) Fe_2B_7, (b) Ru_2B_7 and (c) Os_2B_7. Note that the negative sign only denotes the negative direction corresponding to the positive one.

Open Access Article. Published on 19 September 2017. Downloaded on 11/2/2025 11:16:51 PM.
This article is licensed under a Creative Commons Attribution 3.0 Unported Licence.

Open Access Article. Published on 19 September 2017. Downloaded on 11/2/2025 11:16:51 PM.
This article is licensed under a Creative Commons Attribution 3.0 Unported Licence.

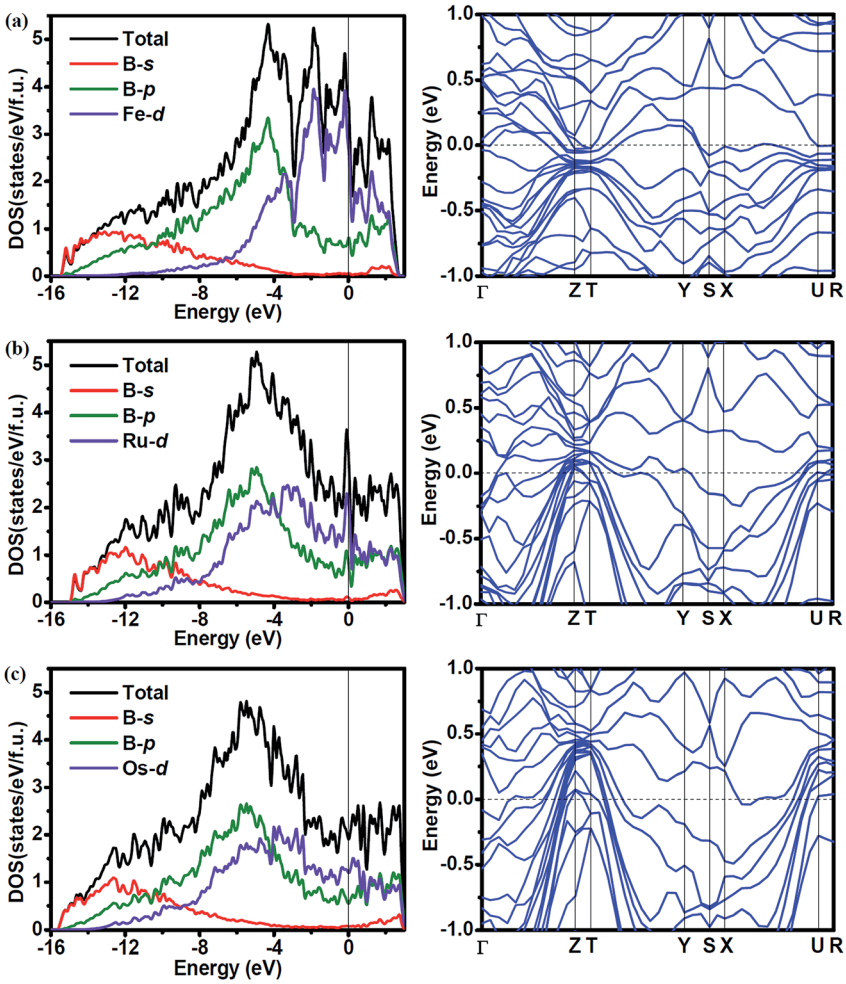

Fig. 4 Density of states (DOS) and band structure for (a) Fe_2B_7, (b) Ru_2B_7 and (c) Os_2B_7.

To gain a more detailed insight into the bonding characters of these compounds, we plot the valence electron density distribution for Fe_2B_7, Ru_2B_7 and Os_2B_7 in (001) and (002) planes in Fig. 5. We can see that there is a charge density maxima located between neighboring B atoms, which correspond to strong directional nonpolar σ covalent B–B bonding. However, between the TM (TM = Fe, Ru and Os) atom and the B atom, the valence electrons are more localized around the B atoms due to the electronegativity difference, corresponding to polar covalent bonding, which mainly originates from the hybridization between TM (TM = Fe, Ru and Os)-d and B-p orbitals.

The relative bond strength between boron atoms can be evaluated by the calculated Mulliken overlap populations (MOP). The bond distances and MOP of B–B bonds in Fe_2B_7, Ru_2B_7 and Os_2B_7 are listed in Table 3. The strongest B–B bond in all three compounds is the B3–B6 bond, which is located in the (001) plane with MOP values of 0.98, 1.00 and 0.94, respectively. The strong B3–B6 bond, nearly parallel to the *b* axis, is responsible for their high incompressibility along this direction. The MOP of B6–B9/B3–B9 is 0.58/0.55 in Fe_2B_7, 0.52/0.49 in Ru_2B_7, and 0.39/0.41 in Os_2B_7, indicating a decrease in the B6–B9/B3–B9 bond strength as TM (TM = Fe, Ru and Os) moves down in group from Fe to Os. A similar trend can be found in the B2–B2 bond, with MOP of 0.68 in Fe_2B_7, only 0.30 in Ru_2B_7, and merely 0.16 in Os_2B_7. For B1–B2, B2–B4 and B2–B8 bonds, MOP is found to be 0.81, 0.46 and 0.90 in Fe_2B_7, 0.87, 0.53 and 0.89 in Ru_2B_7, and 0.83, 0.47 and 0.71 in Os_2B_7. In the (002) plane, MOP for B10–B11, B5–B10 and B5–B11 is between 0.70 and 0.89 in Fe_2B_7, between 0.75 and 0.82 in Ru_2B_7, and between 0.71 and 0.78 in Os_2B_7. As TM (TM = Fe, Ru and Os) moves down in group from Fe to Os, the B13–B14/B7–B12 bond strength decreases, with a MOP value of 0.94/0.8 in Fe_2B_7, 0.91/0.67 in Ru_2B_7, and 0.86/0.46 in Os_2B_7. As for the B7–B14 bond, MOP is found to be 0.53, 0.61 and 0.60 in Fe_2B_7, Ru_2B_7 and Os_2B_7, respectively.

The electron transfer from TM (TM = Fe, Ru and Os) to B atoms is found to be 1.49 *e* for Fe1, 1.61 *e* for Fe2, 1.24 *e* for Fe3 and Fe4 in Fe_2B_7; 1.11 *e* for Ru1, 1.26 *e* for Ru2, 0.85 *e* for Ru3, and 0.93 *e* for Ru4 in Ru_2B_7; 1.02 *e* for Os1, 1.09 *e* for Os2, 0.76 *e* for Os3, and 0.80 *e* for Os4 in Os_2B_7. The valence charge transfer from TM (TM = Fe, Ru and Os) to B atoms indicates the partial ionic character of the TM-B (TM = Fe, Ru and Os) bonds.

 This journal is © The Royal Society of Chemistry 2017

Open Access Article. Published on 19 September 2017. Downloaded on 11/2/2025 11:16:51 PM.
This article is licensed under a Creative Commons Attribution 3.0 Unported Licence.

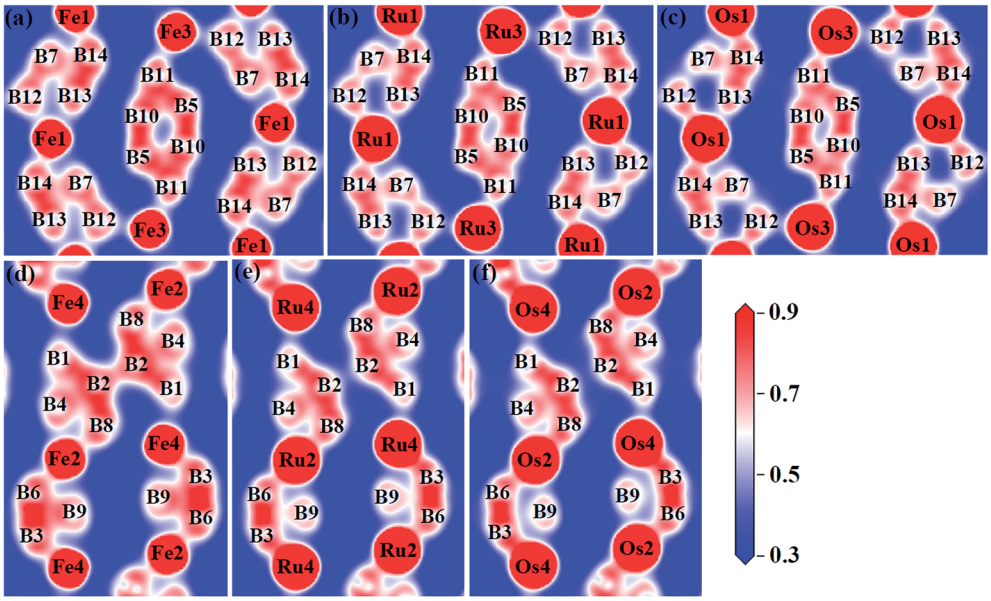

Fig. 5 Valence electron density distribution of (a) Fe_2B_7 in (002) and (d) in (001) planes, (b) Ru_2B_7 in (002) and (e) in (001) planes, (c) Os_2B_7 in (002) and (f) in (001) planes.

Table 3 Bond distances *d* (Å) and MOP of B–B bonds in Fe_2B_7, Ru_2B_7 and Os_2B_7

	Fe_2B_7		Ru_2B_7		Os_2B_7	
	d	MOP	*d*	MOP	*d*	MOP
B3–B6	1.616	0.98	1.644	1.00	1.649	0.94
B13–B14	1.691	0.94	1.733	0.91	1.726	0.86
B2–B8	1.666	0.90	1.692	0.89	1.689	0.71
B10–B11	1.728	0.89	1.800	0.82	1.792	0.78
B1–B2	1.714	0.81	1.740	0.87	1.727	0.83
B7–B12	1.773	0.8	1.884	0.67	1.991	0.46
B5–B11	1.747	0.74	1.800	0.76	1.817	0.72
B5–B10	1.669	0.70	1.682	0.75	1.687	0.71
B2–B2	1.771	0.68	2.117	0.30	2.206	0.16
B6–B9	1.834	0.58	1.991	0.52	2.101	0.39
B3–B9	1.847	0.55	1.986	0.49	2.034	0.41
B7–B14	1.859	0.53	1.884	0.61	1.880	0.60
B2–B4	1.811	0.46	1.838	0.53	1.859	0.47

4 Conclusions

In conclusion, Fe_2B_7, Ru_2B_7 and Os_2B_7 have been studied by first-principles calculations based on density functional theory. Our calculations indicate that the enthalpy of Fe_2B_7 + B is closely similar to that of Fe_2B_8 (FeB_4), which is responsible for the coexistence and the tight mutual intergrowth of the two phases in the experiments. Ru_2B_7 and Os_2B_7 are thermodynamically (Os_2B_7 at 100 GPa) and mechanically stable and can be synthesized experimentally. In addition, the bulk modulus of Fe_2B_7, Ru_2B_7 and Os_2B_7 is higher than that of FeB_4, and the hardness of Fe_2B_7 is comparable to that of FeB_4. The electronic structure calculations indicate that Fe_2B_7, Ru_2B_7 and Os_2B_7 are metallic, which is mainly attributed to the Fe/Ru/Os-d states. The B–B bonding in the three compounds is covalent, and Fe/Ru/Os–B interactions have partial covalent and partial ionic character.

Conflicts of interest

There are no conflicts of interest to declare.

Acknowledgements

This work was supported by the National Natural Science Foundation of China (NSFC) under Grants No. 51201148 and U1530402. L. Wu thanks the foundation of China Postdoctoral Science Foundation (2016M601280). Z. Li thanks Hebei Natural Science Foundation (No. B2015203096) and the Autonomic Research Project of Yanshan University under Grant No. 14LGA017.

References

1 H.-Y. Chung, M. B. Weinberger, J.-M. Yang, S. H. Tolbert and R. B. Kaner, *Appl. Phys. Lett.*, 2008, **92**, 261904.
2 Q. Gu, G. Krauss and W. Steurer, *Adv. Mater.*, 2008, **20**, 3620–3626.
3 M. B. Weinberger, J. B. Levine, H.-Y. Chung, R. W. Cumberland, H. I. Rasool, J.-M. Yang, R. B. Kaner and S. H. Tolbert, *Chem. Mater.*, 2009, **21**, 1915–1921.
4 J. B. Levine, S. H. Tolbert and R. B. Kaner, *Adv. Funct. Mater.*, 2009, **19**, 3519–3533.
5 R. B. Kaner, J. J. Gilman and S. H. Tolbert, *Science*, 2005, **308**, 1268.
6 H.-Y. Chung, M. B. Weinberger, J. B. Levine, A. Kavner, J.-M. Yang, S. H. Tolbert and R. B. Kaner, *Science*, 2007, **316**, 436–439.

Open Access Article. Published on 19 September 2017. Downloaded on 11/2/2025 11:16:51 PM.
This article is licensed under a Creative Commons Attribution 3.0 Unported Licence.

7 J. B. Levine, S. L. Nguyen, H. I. Rasool, J. A. Wright, S. E. Brown and R. B. Kaner, *J. Am. Chem. Soc.*, 2008, **130**, 16953–16958.
8 A. Latini, J. V. Rau, D. Ferro, R. Teghil, V. R. Albertini and S. M. Barinov, *Chem. Mater.*, 2008, **20**, 4507–4511.
9 J. Qin, D. He, J. Wang, L. Fang, L. Lei, Y. Li, J. Hu, Z. Kou and Y. Bi, *Adv. Mater.*, 2008, **20**, 4780–4783.
10 N. Orlovskaya, Z. Xie, M. Klimov, H. Heinrich, D. Restrepo, R. Blair and C. Suryanarayana, *J. Mater. Res.*, 2011, **26**, 2772–2779.
11 R. Mohammadi, A. T. Lech, M. Xie, B. E. Weaver, M. T. Yeung, S. H. Tolbert and R. B. Kaner, *Proc. Natl. Acad. Sci. U. S. A.*, 2011, **108**, 10958–10962.
12 C. Liu, F. Peng, N. Tan, J. Liu, F. Li, J. Qin, J. Wang, Q. Wang and D. He, *High Pres. Res.*, 2011, **31**, 275–282.
13 M. Xie, R. Mohammadi, Z. Mao, M. M. Armentrout, A. Kavner, R. B. Kaner and S. H. Tolbert, *Phys. Rev. B: Condens. Matter Mater. Phys.*, 2012, **85**, 064118.
14 H. Niu, J. Wang, X.-Q. Chen, D. Li, Y. Li, P. Lazar, R. Podloucky and A. N. Kolmogorov, *Phys. Rev. B: Condens. Matter Mater. Phys.*, 2012, **85**, 144116.
15 A. Knappschneider, C. Litterscheid, D. Dzivenko, J. A. Kurzman, R. Seshadri, N. Wagner, J. Beck, R. Riedel and B. Albert, *Inorg. Chem.*, 2013, **52**, 540–542.
16 Y. Wang, T. Yao, L.-M. Wang, J. Yao, H. Li, J. Zhang and H. Gou, *Dalton Trans.*, 2013, **42**, 7041–7050.
17 Q. Li, D. Zhou, W. Zheng, Y. Ma and C. Chen, *Phys. Rev. Lett.*, 2013, **110**, 136403.
18 H. Gou, N. Dubrovinskaia, E. Bykova, A. A. Tsirlin, D. Kasinathan, W. Schnelle, A. Richter, M. Merlini, M. Hanfland and A. M. Abakumov, *Phys. Rev. Lett.*, 2013, **111**, 157002.
19 A. N. Kolmogorov, S. Shah, E. R. Margine, A. F. Bialon, T. Hammerschmidt and R. Drautz, *Phys. Rev. Lett.*, 2010, **105**, 217003.
20 E. Bykova, H. Gou, M. Bykov, M. Hanfland, L. Dubrovinsky and N. Dubrovinskaia, *J. Solid State Chem.*, 2015, **230**, 102–109.
21 S. Deng, J. Zhao, S. Wei, C. Zhu, J. Lv, Q. Li and W. Zheng, *RSC Adv.*, 2016, **6**, 73576–73580.
22 I. Harran, H. Wang, Y. Chen, M. Jia and N. Wu, *J. Alloys Compd.*, 2016, **678**, 109–112.
23 R. Yu, Q. Zhan and X.-F. Zhang, *Appl. Phys. Lett.*, 2006, **88**, 051913.
24 B. Aronsson, *Acta Chem. Scand.*, 1963, **17**, 2036–2050.
25 R. B. Roof Jr and C. P. Kempter, *J. Chem. Phys.*, 1962, **37**, 1473–1476.
26 R. Yu, Q. Zhan and L. C. De Jonghe, *Angew. Chem., Int. Ed.*, 2007, **46**, 1136–1140.
27 K. Niwa, K. Suzuki, S. Muto, K. Tatsumi, K. Soda, T. Kikegawa and M. Hasegawa, *Chem.–Eur. J.*, 2014, **20**, 13885–13888.
28 Y. X. Wang, M. Arai, T. Sasaki and C. Z. Fan, *Phys. Rev. B: Condens. Matter Mater. Phys.*, 2007, **75**, 104110.
29 S. J. Clark, M. D. Segall, C. J. Pickard, P. J. Hasnip, M. I. J. Probert, K. Refson and M. C. Payne, *Z. Kristallogr.*, 2005, **220**, 567–570.
30 J. P. Perdew, K. Burke and M. Ernzerhof, *Phys. Rev. Lett.*, 1996, **77**, 3865.
31 H. J. Monkhorst and J. D. Pack, *Phys. Rev. B: Solid State*, 1976, **13**, 5188.
32 R. Hill, *Proc. Phys. Soc., London, Sect. A*, 1952, **65**, 349.
33 X.-Q. Chen, H. Niu, D. Li and Y. Li, *Intermetallics*, 2011, **19**, 1275–1281.
34 Y. Tian, B. Xu and Z. Zhao, *Int. J. Refract. Met. Hard Mater.*, 2012, **33**, 93–106.
35 S. Rundquist and N. O. Ersson, *Ark. Kemi*, 1968, **30**, 103.
36 A. Kjekshus and G. Pedersen, *Acta Crystallogr.*, 1961, **14**, 1065–1070.
37 Z.-J. Wu, E.-J. Zhao, H.-P. Xiang, X.-f. Hao, X.-j. Liu and J. Meng, *Phys. Rev. B: Condens. Matter Mater. Phys.*, 2007, **76**, 054115.
38 Z. Wu and J. Meng, *Comput. Mater. Sci.*, 2008, **43**, 495–500.
39 Y. Zhang, L. Wu, B. Wan, Y. Zhao, R. Gao, Z. Li, J. Zhang, H. Gou and H.-k. Mao, *Phys. Chem. Chem. Phys.*, 2016, **18**, 2361–2368.
40 L. Wu, B. Wan, Y. Zhao, Y. Zhang, H. Liu, Y. Wang, J. Zhang and H. Gou, *J. Phys. Chem. C*, 2015, **119**, 21649–21657.
41 M. Yang, Y. C. Wang, J. L. Yao, Z. P. Li, J. Zhang, L. L. Wu, H. Li, J. W. Zhang and H. Y. Gou, *J. Solid State Chem.*, 2014, **213**, 52–56.
42 S. F. Pugh, *Philos. Mag.*, 1954, **45**, 823–843.
43 J. Haines, J. M. Leger and G. Bocquillon, *Annu. Rev. Mater. Res.*, 2001, **31**, 1–23.
44 J. F. Nye, *Physical properties of crystals*, Oxford university press, 1985.

 This journal is © The Royal Society of Chemistry 2017